

---

# Towards Semantic Equivalence of Tokenization in Multimodal LLM

---

Shengqiong Wu<sup>1,2\*</sup>, Hao Fei<sup>1,2†</sup>, Xiangtai Li<sup>2</sup>, Jiayi Ji<sup>1</sup>,  
Hanwang Zhang<sup>2,3</sup>, Tat-Seng Chua<sup>1</sup>, Shuicheng Yan<sup>2</sup>  
<sup>1</sup>National University of Singapore, <sup>2</sup>Skywork AI, Singapore,  
<sup>3</sup>Nanyang Technological University

## Abstract

Multimodal Large Language Models (MLLMs) have demonstrated exceptional capabilities in processing vision-language tasks. One of the crux of MLLMs lies in vision tokenization, which involves efficiently transforming input visual signals into feature representations that are most beneficial for LLMs. However, existing vision tokenizers, essential for semantic alignment between vision and language, remain problematic. Existing methods aggressively fragment visual input, corrupting the visual semantic integrity. To address this, this paper proposes a novel dynamic Semantic-Equivalent Vision Tokenizer (**SeTok**), which groups visual features into semantic units via a dynamic clustering algorithm, flexibly determining the number of tokens based on image complexity. The resulting vision tokens effectively preserve semantic integrity and capture both low-frequency and high-frequency visual features. The proposed MLLM (**SETOKIM**) equipped with SeTok significantly demonstrates superior performance across various tasks, as evidenced by our experimental results. The project page is at <https://chocowu.github.io/SeTok-web/>.

## 1 Introduction

Recently, the research on Multimodal Large Language Models (MLLMs) has garnered intense interest [99, 54, 19, 88]. By building upon the unprecedented intelligence of language-based LLMs [15, 87], and integrating multimodal encoders [71] at the input side and decoders [76] at the output side, current MLLMs have developed powerful multimodal capabilities. Particularly, in the visual modality, the state-of-the-art (SoTA) MLLMs have now achieved a grand slam across the four major visual-language task groups, i.e., understanding [91, 2, 18], generating [52, 72, 100], segmenting [49, 39, 92], and editing [16, 102, 7]. Central to this capability is the design of vision tokenization [21, 24], which concerns how to effectively transform input visual signals into feature representations that are most conducive to being understood by LLMs. Specifically, existing vision tokenizers can be mainly categorized into two types: 1) tokenization via image patchifying (cf. Fig. 1(a)), and 2) tokenization via codebooks (cf. Fig. 1(b)).

While SoTA MLLMs have achieved promising performances across various tasks, a significant bottleneck remains with current visual tokenization methods, i.e., resulting in insufficient semantic alignments between language and vision tokens. On the language side, linguistic tokens (or words) are naturally discrete, representing well-encapsulated semantic units, whereas, on the vision side, visual pixels are inherently continuous data with no physical boundaries. Intuitively, language tokens should correspond to semantically encapsulated objects (or compositional regions) within an image. For instance, when “a dog” is mentioned, the “dog” token should correspond to the exact pixel region

---

\*Work is done as an intern at Skywork AI.

†Corresponding author.

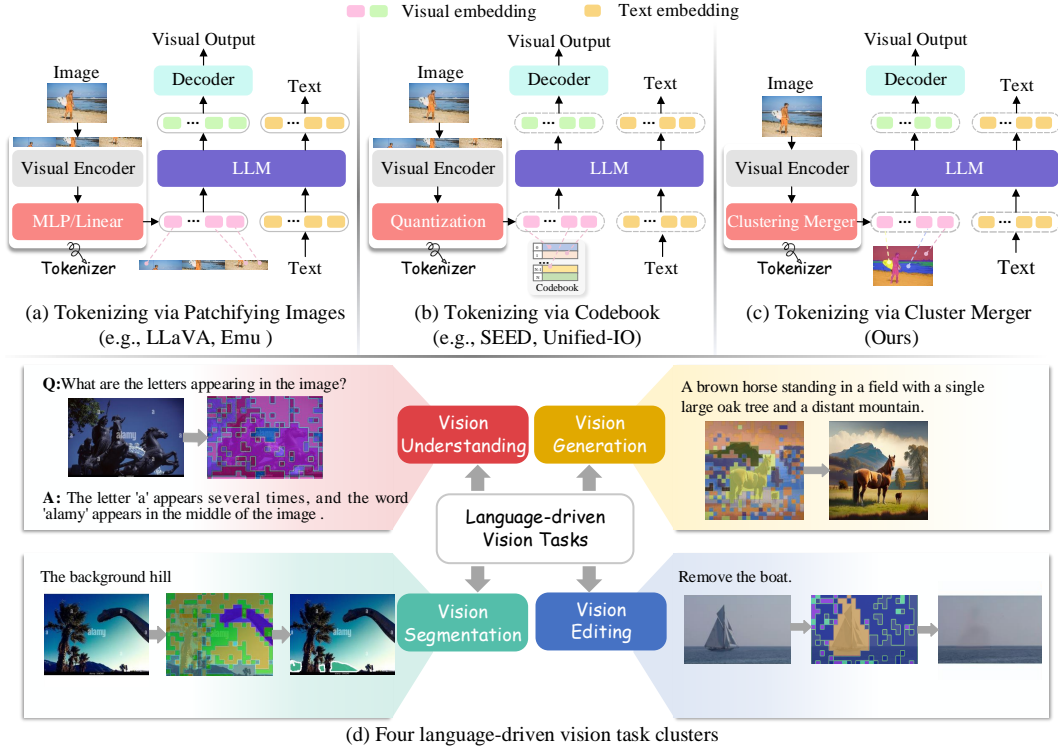


Figure 1: Comparisons between existing MLLMs in tokenizing input image via (a) Patchifying image, (b) Codebook, and (c) Cluster Merger. In (d), we show four language-driven vision tasks enhanced with semantic-equivalent vision tokens where regions with the same color denote a vision token.

of the dog in the image. However, as illustrated in Fig. 1(a&b), both existing tokenization methods via image patchifying or codebooks divide the image into fixed patch squares, causing objects within the image to be split across different patches, thus disrupting the integrity of visual semantic units. This semantic fragmentation further might largely lead to the loss of high-frequency visual information, e.g., the object’s edges and lines. Ultimately, this misalignment between vision and language within MLLMs undermines the effective understanding of visual signals, significantly hindering progress in a range of vision-language tasks that require precise, fine-grained semantic alignment between vision and language elements.

To this end, this work proposes a Semantic-Equivalent Tokenizer (**SeTok**) for enhancing visual MLLMs, where we encourage the vision and language tokens to be semantically congruent. The core idea involves automatically grouping visual features from input images by applying a clustering algorithm [23], such that each unique cluster represents an encapsulated semantic unit within the vision. As illustrated in Figure 1(c), the red visual area aggregated by SeTok corresponds to a complete semantic concept—“*person*”, while the yellow area corresponds to the “*surface board*” concept. Furthermore, we recognize that tokenizing images into a fixed number of patches is impractical. From a semantic perspective, different images should contain varying numbers of semantically encapsulated objects, and the granularity of compositional regions also needs to be flexibly determined. For example, we only need to identify a person in the image, while at other times, we may need to delineate the person’s head precisely. This implies that it is more reasonable to determine the division of visual tokenization dynamically. To address this, we propose a dynamic clustering mechanism [23] that iteratively determines cluster centers based on density peaks, assigning visual features to these centers until all features are allocated. The design of this mechanism allows for the dynamic determination of the number of concept visual tokens, rather than fixing the ratio [35] or merely merging the top- $k$  visual tokens [5]. Next, after clustering, we devise a cluster merger to aggregate the visual features within each cluster, that is dedicated to learning a complete visual semantic unit feature, including both high-frequency and low-frequency information.

We further build an MLLM equipped with our SeTok, named **SETOKIM**. Then, through pre-training and instruction-tuning on the multimodal data across diverse tasks (e.g., text-to-image generation,

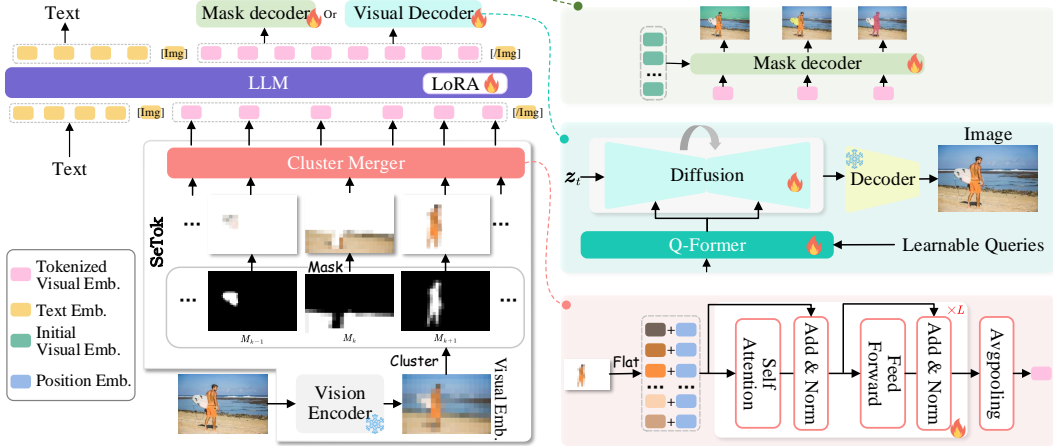


Figure 2: The overview of SETOKIM. The visual embedding extracted from a vision encoder is tokenized into vision tokens by **SeTok**, combined with text tokens to be input LLM for vision-language understanding. The output vision embeddings from LLM are fed into a vision decoder and mask decoder to generate realistic images and semantic segmentation masks, respectively.

image editing, image QA), our model evolves into a versatile multimodal generalist and excels in all task groups demonstrated by extensive experiments, as shown in Figure 1(d). Compared with other methods that focus on vision tokenization, in-depth analyses reveal that **SeTok** enjoys the superiority of tokenizing vision input into more interpretable and semantic-complete vision tokens, achieving the enhancement of vision-language alignment. Moreover, SeTok can also be easily integrated into established MLLMs with minimal adaptation. Extensive experiments reveal that this integration significantly boosts task performance, meanwhile keeping stronger interpretability, and also reducing training costs and inference time.

## 2 Methodology

In this work, we aim to generate semantically complete and the least-loss vision tokens aligned with text tokens to facilitate fine-grained semantic interactions between vision and language, thereby enhancing the performance of MLLMs in various multimodal tasks. In pursuit of this goal, we propose constructing a semantic-equivalent tokenizer, which takes visual features extracted from a well-trained vision encoder as input and outputs semantically complete visual tokens, as illustrated in Figure 2. Coupled with the vision tokenizer, the vision input can be tokenized into semantically equivalent tokens to the text, which are then fed into the LLM together with the text tokens.

### 2.1 Semantic-equivalent Vision Tokenizer

Given an input image  $I \in \mathbb{R}^{H \times W \times 3}$ , we first employ a vision encoder to extract a sequence of visual embeddings  $\mathbf{X} = \{x_{i,j}\} \in \mathbb{R}^{h \times w \times d}$ , where  $d$  is the embedding dimension<sup>3</sup>. Then, to obtain semantically complete visual tokens, we propose to amalgamate the visual features into several clusters based on semantic similarity.

**Vision Cluster.** We take the visual embeddings as input, which are then clustered into a variable number of attention masks  $\mathbf{M} \in \mathbb{R}^{h \times w \times k}$ , which assign individual visual embedding to object-like scene components. Inspired by [23], this is intuitively achieved by (1) selecting the location  $(i, j)$  of the visual feature that has not yet been assigned to a cluster, (2) creating a cluster assignment according to the distance of the embeddings at the selected pixel location to all other embeddings according to a distance kernel  $\varphi$ <sup>4</sup>, and (3) repeating the first two steps until all visual embeddings are accounted for or a stopping criterion is met. Different from [22] employing uniformed seed scores performing the stochastic selection of visual embeddings, we propose to choose the visual embeddings based on their density peaks, as a higher density shows a higher potential to be the cluster center. Specifically, we first calculate the local density  $\rho_{i,j}$  of the token  $x_{i,j} \in \mathbf{X}$  by referring its

<sup>3</sup>When using ViT-based vision encoder,  $h = \frac{H}{p}$ ,  $w = \frac{W}{p}$ , where  $p$  is the patch size. Similarly, when using a CNN-based encoder,  $h$  and  $w$  are the sizes of the feature map obtained by the convolutional neural network.

<sup>4</sup>In this work, we employ  $\varphi = \exp(-\|\mathbf{u} - \mathbf{v}\|^2 \cdot k \ln 2)$

neighbors:

$$\rho_{i,j} = \exp\left(-\frac{1}{K} \sum_{\mathbf{x}_{m,n} \in \text{KNN}(\mathbf{x}_{i,j}, \mathbf{X})} \|\mathbf{x}_{m,n} - \mathbf{x}_{i,j}\|^2\right), \quad (1)$$

where  $\text{KNN}(\mathbf{x}_{i,j}, \mathbf{X})$  denotes the  $K$ -nearest neighbors of  $\mathbf{x}_{i,j}$  in  $\mathbf{X}$ . We then measure the minimal distance  $\delta_{i,j}$  between the feature  $\mathbf{x}_{i,j}$  and other features with higher density:

$$\delta_{i,j} = \begin{cases} \min_{m,n: \rho_{m,n} > \rho_{i,j}} \|\mathbf{x}_{i,j} - \mathbf{x}_{m,n}\|^2, & \text{if } \exists m, n : \rho_{m,n} > \rho_{i,j} \\ \max_{m,n} \|\mathbf{x}_{i,j} - \mathbf{x}_{m,n}\|^2, & \text{otherwise} \end{cases} \quad (2)$$

Finally, we summarize the score  $s_{i,j}$  of the feature by combining the local density  $\rho_{i,j}$  and minimal distance  $\delta_{i,j}$  as  $\rho_{i,j} \times \delta_{i,j}$ . Based on the score, we select the location  $(i, j)$  of the visual feature that has the highest score  $s_{i,j}$  and has not yet been assigned to a cluster, and iteratively assign the visual feature into a certain cluster until a stopping condition is satisfied, at which point the final scope is added as an additional mask to explain any remaining visual embeddings. The detailed process is described formally in Appendix §C.

**Cluster Merger.** After clustering, the visual embeddings are grouped based on the attention masks  $M$ . To retain information within each cluster optimally, we adopt a cluster merger that aggregates visual embeddings beyond merely using cluster centers as definitive vision tokens. This merger consists of  $L$  stacked blocks, each containing a self-attention layer, a residual and normalization layer, and a feed-forward layer. In addition, considering the significance of positional information for representing a semantic concept in an image, we integrate 2D position embeddings (PE, [32]) into the merger, calculated as  $\hat{X}_i = \text{PE}(\mathbf{X}) \odot M_i + \mathbf{X} \odot M_i$ . The cluster features are then flattened into a sequence  $\hat{X}_i = \{\mathbf{x}_i\} \in \mathbb{R}^{N \times d}$  in raster-scan order, where  $N$  is the number of the visual features within a cluster. Subsequent processing involves applying average pooling across the visual features within a cluster to obtain the final cluster feature  $\mathbf{u}_i = \text{Avg}(\text{Merger}(\hat{X}_i)) \in \mathbb{R}^d$ . Consequently, our tokenizer can tokenize the input vision into a variable number of semantic tokens  $\mathbf{U} = \{\mathbf{u}_i\} \in \mathbb{R}^{k \times d}$ .

## 2.2 Multimodal Training Scheme

In this work, we consider a three-stage training procedure. It can be summarized as follows. The implementation details, like training data, can be found in Table 7 in Appendix §D.

**Stage-I: Tokenizer Pretraining.** This stage aims to truly endow the tokenizer with the capability of tokenizing the input vision into a semantic complement and independent tokens that can capture the low-frequency semantic features and high-frequency pixel features. Therefore, we employ a vision decoder to decode realistic images by taking the tokenized visual tokens as inputs. Specifically, the vision tokens obtained from the tokenizer are fed into a learnable feature mapper (i.e., Q-former [45]) module as the inputs of the U-Net  $\epsilon_\theta$  [76] to infill the visual details, where the learnable module consists of four cross-attention layers to connect the visual tokenizer and the U-Net. Following [76], the parameters  $\theta$  of this U-Net are optimized by  $\epsilon$  prediction:

$$\mathcal{L}_{unet} = \mathbb{E}_{\epsilon \sim \mathcal{N}(0,1), t, \mathbf{z}_t, \mathbf{U}} [\|\epsilon - \epsilon_\theta(\mathbf{z}_t, t, \mathbf{U})\|_2^2], \quad (3)$$

where  $\epsilon$  is the unscaled noise,  $t$  is the sampling step,  $\mathbf{z}_t$  is latent noise at step  $t$ . In addition, an accurate tokenizer should be equipped with precise delineation of the boundaries between tokens, i.e., the accuracy of the clustering. Meanwhile, we observe that attention masks correlate with object masks, but they often fail to align precisely with actual object boundaries. We conjecture that this misalignment stems from the vision encoder’s tendency to spatially dilate information about objects, thus obscuring precise boundary delineation. Consequently, we introduce to incorporate a mask decoder [48] taking the vision tokens as input to decode the object mask. We follow [48] to use binary cross-entropy loss  $\mathcal{L}_{bce}$  and dice loss  $\mathcal{L}_{dice}$  to compute the loss for masks. Moreover, we encompass an auxiliary mask consistency loss designed to encourage greater similarity between the cluster results and the object masks  $\pi$ , thereby enhancing their alignment.

$$\mathcal{L}_{mask} = \text{KL}(M \parallel \text{nograd}(\pi)) + \mathcal{L}_{bce} + \mathcal{L}_{dice}, \quad (4)$$

where  $\pi \in [0, 1]^{h \times w \times k}$  are a set of the object masks, and  $\sum_n \pi_{i,j,n} = 1$ .

Overall, the training of the tokenizer involves two sub-phases: 1) in the first sub-phrase, we freeze the vision encoder and focus solely on training the learnable components, which include the cluster merger, the q-former, and keys and values within the U-Net. This stage is conducted with 50k training steps using datasets such as CC3M [80] and LAION-AESTHETICS [77]. 2) in the second sub-phrase, we integrate a mask decoder to encourage fine-grained object boundary learning. This extended training is performed on the MSCOCO 2017 [55] and SAM-1B [38] datasets.

Method	Size	Image Caption			Image QA					
		NoCaps	Flickr30K	VQA <sup>v2.0</sup>	OK-VQA	GQA	VSR	IconQA	VizWiz	TextQA
BLIP-2 [92]	13B	98.4	73.7	65.0	-	41.0	-	-	19.6	42.5
InstructBLIP [56]	7B	-	-	49.2	-	-	34.5	50.1	-	-
InstructBLIP [56]	13B	120.0	83.5	-	-	49.5	-	-	33.4	50.7
Emu-1 [98]	7B	106.8	80.9	57.5	46.2	46.0	53.9	42.9	38.1	67.0
DreamLLM [20]	7B	-	-	34.8	45.2	36.0	-	-	-	-
SEED [29]	7B	90.4	66.7	-	-	34.8	45.2	36.0	-	-
LaVIT [36]	7B	114.2	83.0	66.0	54.6	46.8	-	-	38.5	-
Shikra [11]	13B	-	-	77.4*	-	-	-	-	-	-
LLaVA-1.5 [58]	7B	-	-	78.5*	-	62.0*	-	-	50.0	58.2
LLaVA-1.5 [58]	13B	-	-	80.0*	-	63.3*	-	-	53.6	61.3
Qwen-VL [3]	13B	-	-	78.8*	-	59.3*	-	-	35.2	63.8*
Yi-VL [94]	6B	-	-	75.1*	56.9*	58.4*	60.4	47.6	50.0	-
MiniGPT-v2-chat [10]	7B	-	-	-	57.8*	60.1	62.9	51.5	53.6	-
<b>SETOKIM</b>	7B	123.5	86.5	79.6*	58.7*	64.4*	63.4	54.1	58.1	60.5
<b>SETOKIM</b>	13B	<b>124.0</b>	<b>87.2</b>	<b>83.9*</b>	<b>60.2*</b>	<b>67.2*</b>	<b>66.5</b>	<b>55.7</b>	<b>59.6</b>	<b>65.3</b>
SoTA Specialist	-	-	-	86.1*	66.1*	94.7*	70.1*	82.6*	73.3*	71.4*
				[13]	[13]	[53]	[85]	[64]	[14]	[13]

Table 1: Comparison between different MLLMs on image understanding benchmarks. \* denotes the corresponding training sets utilized for SETOKIM instruction-tuning.

**Stage-II: Multimodal Pretraining.** In this phase, we enhance the LLM to possess interleaved understanding and generation capabilities for vision-language tasks. Thus, on the one hand, we adopt next-token prediction-based cross-entropy loss for the textual content generation. Meanwhile, we employ embedding regression loss to train LLM to generate visual tokens, which are trained to reconstruct the features on the pre-trained vision tokenizer with a Mean Squared Error (MSE) loss. We add two special tokens ‘[Img]’ and ‘[/Img]’ to represent the beginning and the end of the query embeddings, and the ‘[Img]’ is trained to predict where an image emerges. We pre-train the LLM initialized from Vicuna-v1.5 [15] on massive multimodal data, including 558K image-caption pairs from the LLaVA-filtered CC3M dataset [58] and 695K sampled GPT-4V-responded captions from the ALLaVA dataset [9]. In addition, we pretraining our model with the image-editing dataset, i.e., InstructPix2Pix [6], to enable the model to perform vision editing.

**Stage-III: Instruction Tuning.** We perform multimodal instruction tuning through fine-tuning LLM using a LoRA [33] module with both public datasets covering fine-grained visual QA, image generation and editing, and text-rich grounded datasets. Following [58], we utilize 665K single- and multi-turn conversations from the LLaVA-150K [59], ShareGPT4V [12], academic-task-oriented VQA datasets (e.g., VQA<sup>v2</sup>[30], GQA [34], OK-VQA [67], A-OKVQA [78]), and region-level perception (e.g., Visual Genome [42], RefCOCO [37]), to enhance the model’s vision understanding capabilities. Furthermore, we generate prompts that produce or edit images suitable for the conversation context, bringing 15K image-related generation and editing pairs based on the InstructPix2Pix dataset for image-related generation and editing. Appendix §D provides more training details.

### 3 Experiments and Analysis

In the experiments, we aim to quantify the performance of SETOKIM across various vision-language tasks primarily compared to MLLMs([20, 40, 63, 50, 82, 83]) focus on visual comprehension and generation, as well as with widely-used MLLMs ([58, 3, 45, 17]) that specialize in segmentation or editing. Appendix §D details experimental setups and implementation specifics.

#### 3.1 Main Results

**Visual Understanding.** We first evaluate our model across a wide range of academic benchmarks, including image captioning and image QA datasets. As depicted in Table 1, our model achieves competitive performance in various vision-understanding tasks. Specifically, in the captioning tasks, our model outperforms both the specialist InstructBLIP and the previous SoTA MLLMs, LaVIT, and SEED, by achieving the highest CIDEr score. Moreover, our model demonstrates superior performance on various QA datasets, notably improving GQA by 3.9% and iconQA by 4.2%, suggesting that our approach has a distinct advantage in understanding the relationships and quantities between objects. Further, across various MLLM benchmarks shown in Table 2, our model consistently exhibits higher performance, underscoring its robust multimodal comprehension capabilities and mitigating the hallucination issues.

**Referring Expression Segmentation.** Table 3 presents various MLLMs’ performances on referring expression segmentation tasks. It is noteworthy that our model consistently outperforms the baselines,



Method	POPE	MME	MMB <sup>en</sup>	MM-Vet	Method	refCOCOg		refCOCO+		Reaseg	
						val(U)	test(U)	val	testA	testB	gIoU cIoU
BLIP-2-13B [45]	85.3	1293.8	-	-	ReLA [56]	65.0	66.0	66.0	71.0	57.7	- -
InstructBLIP-13B [17]	78.9	1212.8	-	-	SEEM [104]	65.7	-	-	-	-	24.3 18.7
Qwen-VL-Chat [3]	-	1487.5	60.6	-	PixelLM [75]	69.3	70.5	66.3	71.7	58.3	- -
LLaVA-1.5-7B [58]	-	809.6	64.3	31.1	NExT-Chat [97]	67.0	67.0	65.1	<b>71.9</b>	56.7	- -
LLaVA-1.5-13B [58]	85.9	1510.7	67.7	36.1	LISA [43]	67.9	70.6	65.1	70.8	58.1	47.3 48.4
Unified-IO 2xxl [63]	87.7	1500.1	<b>71.5</b>	-	<b>SETOKIM</b>	<b>70.9</b>	<b>71.5</b>	<b>67.4</b>	71.3	<b>61.2</b>	<b>49.4 53.7</b>
DreamLLM-7B [19]	-	-	49.9	35.9							
Mini-Gemini-13B [50]	-	1565.0	68.5	46.0							
<b>SETOKIM (13B)</b>	<b>89.1</b>	<b>1578.5</b>	69.8	<b>48.7</b>							

Table 2: Comparison on POPE [51], MME [25], segmentation benchmarks. We report cIoU for MMB [61], MM-Vet [95].

Table 3: Results on 3 referring expression segmentation benchmarks. We report cIoU for RefCOCO+/g.

Method	MS-COCO-30K		MagicBrush		Emu-Edit		EVR	
	FID ↓	CLIP <sub>im</sub> ↑	CLIP <sub>im</sub> ↑	L <sub>1</sub> ↓	CLIP <sub>im</sub> ↑	L <sub>1</sub> ↓	CLIP <sub>im</sub> ↑	L <sub>1</sub> ↓
<b>• Diffusion-based Method</b>								
InstructPix2Pix [7]	-	-	83.4	12.1	35.9	17.6	81.4	18.9
MagicBrush [102]	-	-	83.8	10.0	-	-	-	-
SD [76]	12.6	-	-	-	-	-	-	-
<b>• MLLM-based Method</b>								
MGIE [26]	-	-	<b>91.1</b>	8.2	-	-	81.7	16.3
GILL [40]	12.2	67.5	75.2	28.3	-	-	65.0	31.8
Emu-1[98]	11.6	66.5	78.5	27.9	-	-	69.2	30.7
Emu-2-gen [82]	-	68.6	85.7	19.9	-	-	80.3	22.8
SEED [29]	-	68.2	80.9	24.5	-	-	72.3	28.4
<b>SETOKIM</b>	<b>8.5</b>	<b>69.8</b>	90.7	<b>5.7</b>	<b>87.2</b>	<b>8.5</b>	<b>83.5</b>	<b>15.1</b>

Table 4: Performance of various models in zero-shot text-to-image generation and editing on the MS-COCO-30K, MagicBrush, Emu-Edit, and EVR evaluation benchmarks.

and significantly surpasses the current SoTA on the ReaSeg dataset, demonstrating the proficiency of our vision tokens derived from **SeTok** in capturing not only object-centric low-frequency semantic details but also the high-frequency boundary details.

**Visual Generation and Editing.** We next evaluate our model’s effectiveness in vision generation and editing. Table 4 demonstrates that images generated by our model consistently show higher similarity to ground-truth images compared with other MLLMs, highlighting superior vision-text translation. Further, we test our model in instruction-based image editing on MagicBrush [101], Emu-Edit [81], and EvR [86]. Standard pixel difference (L1) and visual feature similarity (CLIP<sub>im</sub>) are employed as metrics. It can be observed that compared to diffusion-based specialists, our model enjoys a higher performance. In addition, our model also demonstrates distinct superiority in terms of L1 and CLIP scores compared to existing MLLMs. Compared to Emu or SEED, which tokenize images into semantic fragments leading to the neglect of the high-frequency details in images, our model shows a greater advantage in L1 scores, indicating robust capabilities of our vision tokens in both textual interpretation and high-fidelity image generation.

### 3.2 In-depth Analysis

#### The Impact of the Clustering Mechanism.

Here, we compare the impact of different clustering mechanisms on model performance, w.r.t, training time, computational overhead, and zero-shot performance on multimodal understanding tasks. As shown in Table 5, we can observe that tokenizers constructed using dynamic clustering mechanisms achieve superior overall performance compared to those with a fixed setup while simultaneously accelerating training time and reducing computational costs during inference. Specifically, we note that using a pre-defined threshold to dynamically determine the number of clusters can lead to variations in the threshold due to score inconsistencies, resulting in poor generalization across different datasets.

Mechanism	#Cluster	TFLOPs	Flickr30K	OK-VQA
Threshold	19*	7.8	84.6	57.8
Hard-clustering	25*	8.1	87.2	60.2
Soft-clustering	23*	8.3	86.7	58.9
	576	15.5	83.4	52.1
Fixed	256	13.7	85.1	51.7
	64	10.9	84.1	53.6
	8	10.1	84.4	50.1
Resampler [1]	64	10.1	83.4	54.5

Table 5: The effect of different clustering strategies. The first three rows consist of dynamic strategies. #Cluster is the number of clusters, and \* denotes the average cluster number.

In contrast to soft-clustering, which yields soft

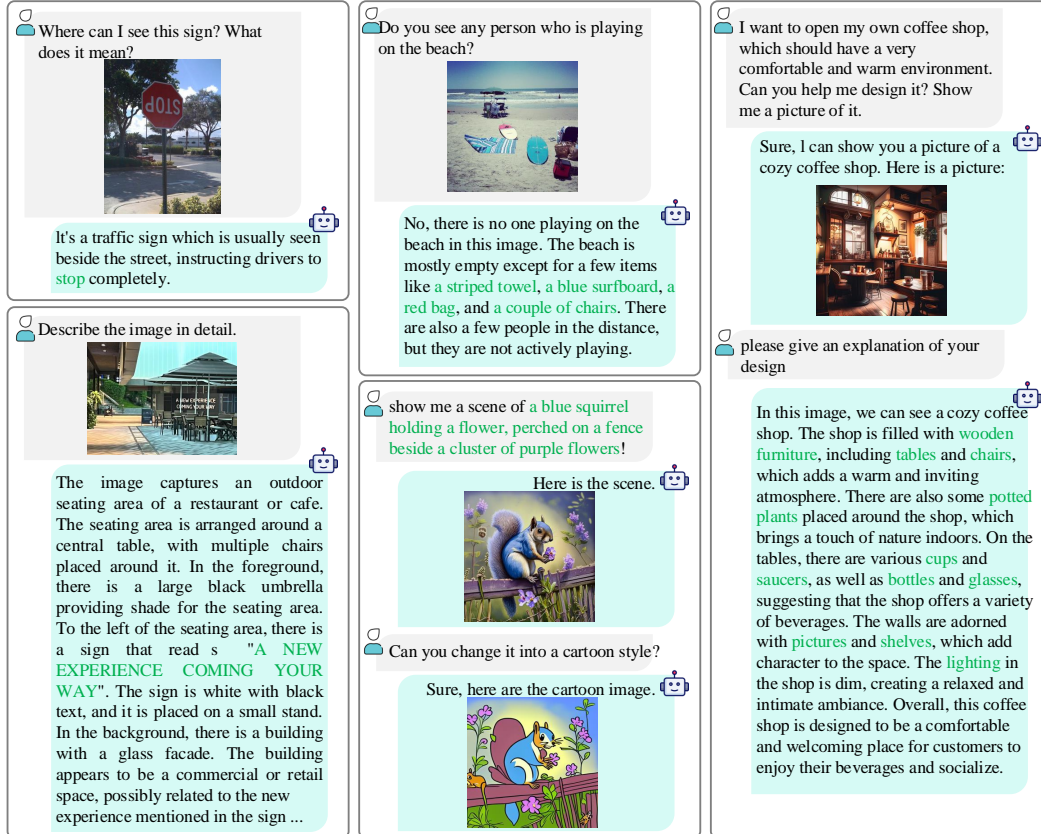


Figure 3: Qualitative results on image understanding and generation. The words marked in green are key elements in questions and answers.

attention masks, our findings suggest that hard-clustering produces better results, as it may be because hard clustering leads to higher consistency of cluster outcomes [31], leading to more stable visual tokens and enhancing both the stability and performance of the model. When employing a fixed number of clusters, the key challenge is to determine the optimal number of clusters. As shown in Table 5, different datasets achieve optimal performance at varying numbers of clusters, with a uniform count across all datasets, resulting in suboptimal outcomes. Furthermore, we compare our mechanism to the current resampler approach [1], in which a fixed number of queries are used to group features via a cross-attention mechanism. Our experiments reveal that dynamic clustering still enjoys the superiority in multimodal understanding, likely because the fixed query tokens are not truly aligned with the number of semantic units in visual content and is essentially a soft cluster method.

**Qualitative Analysis of Visual Understanding and Generation.** As illustrated in Figure 3, our model exhibits proficiency in intricate image understanding tasks, such as deciphering reversed text, exemplified by the word “stop”, and accurately identifying text “A NEW EXPERIENCE COMING YOUR WAY” that is partially covered. In tasks involving detailed image descriptions, our approach prioritizes object-level information within images, which substantially mitigates the incidence of hallucinatory responses commonly observed in MLLMs. Moreover, in text-to-image generation, our model demonstrates remarkable capabilities in synthesizing coherent images, which maintain a high degree of fidelity and relevance to the textual context, such as the “flower”, “fence” and “squirrel”.

**Qualitative Analysis of Visual Segmentation.** We present the segmentation examples in Figure 4. It is easy to note that the attention mask closely aligns with the object mask, and our model shows superiority in achieving more accurate and detailed segmentation results compared to other LLM-based segmentation methods. Notably, as depicted in the second row of the figure, the visual token generated by our method encompasses all depicted fish, effectively achieving a complete segmentation of the fish in the scene. In contrast, other models produce only partial segmentation. This effectiveness of the segmentation highlights the precise content representation and improved

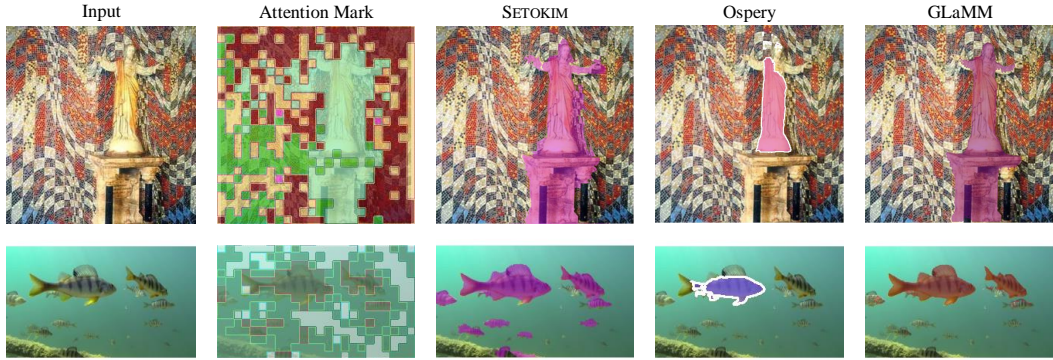


Figure 4: The visualizations for segmentation results compared with GLaMM[74] and Ospery [96].

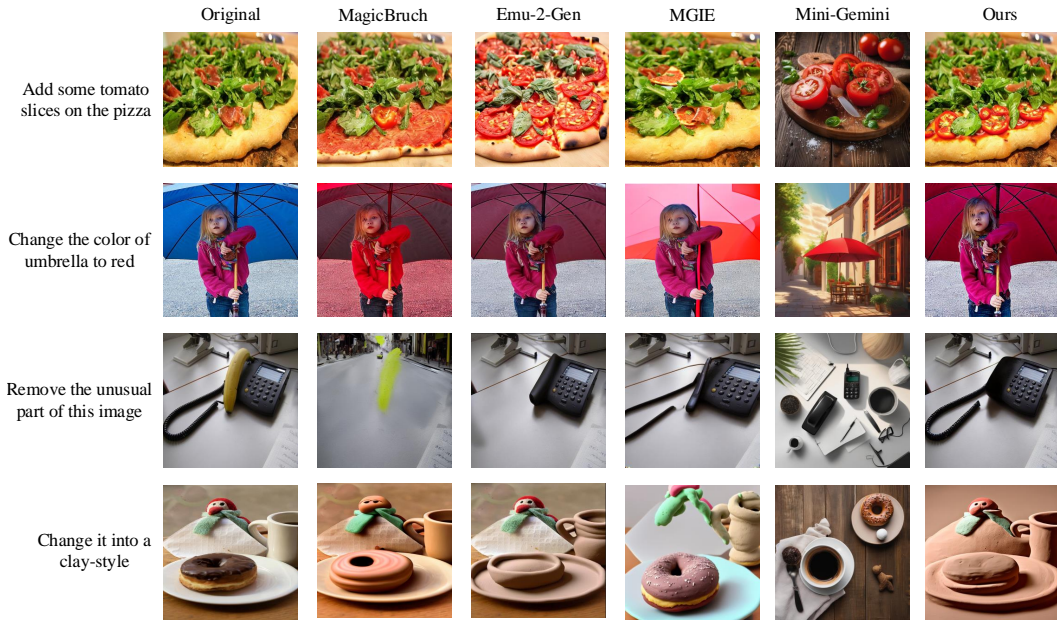


Figure 5: Qualitative comparison between MLLMs for the image editing. SETOKIM excels in adhering to instructions and preserving low-level image details.

interpretability of the visual tokens. Such visual tokens eventually enhance the vision-language understanding incorporated with the text tokens.

**Qualitative Analysis of Visual Editing.** Here, we evaluate the efficacy of image manipulation using our model compared to the previous diffusion-based method MagicBrush [101], and various MLLMs including Emu-2-Gen [82], MGIE [26], and Mini-Gemini [50]. As depicted in Figure 5, SETOKIM displays superior performance by closely adhering to the provided instructions and preserving intricate image details. For instance, our model seamlessly adds ‘tomato slices’ to an image without altering other elements on the pizza, while Emu-2-Gen and MGIE fall short. Furthermore, our model exhibits remarkable precision in changing the color of an umbrella while visual objects not intended for alteration retain a high level of consistency before and after editing. Additionally, SETOKIM demonstrates to precisely follow implicit user instructions to remove unusual elements from an image, i.e., the banana, preserving the surrounding context, whereas Emu-2-Gen mistakenly removes a telephone cord and MGIE fails to remove the banana properly, altering the cord’s texture. These examples underscore the effectiveness of SETOKIM for high-precision image manipulation, leveraging semantically equivalent visual tokens to achieve nuanced and context-aware results.

**Qualitative Analysis of Visual Tokens.** In Figure 6, we demonstrate how input visual features are assigned to visual tokens after tokenization. Firstly, we observe that our tokenization method during clustering bears a resemblance to partial segmentations representing semantic complete units. For instance, in the first and second images 1 and 2, a person is represented as a single token;





Figure 6: The visualizations for visual tokens.

however, in the third image, the person is segmented into different tokens for the head and body. This segmentation is similar to the fifth image, where a baby is divided into distinct tokens for the hair, face, body, and hands. Furthermore, in scenarios involving multiple instances of the same class, such as the two persons in the final image, identical parts from all instances are amalgamated. This approach ensures that similar visual features across different entities are recognized and processed collectively, enhancing the coherence and efficiency of our model’s tokenization process.

## 4 Related Work

Currently, benefiting from the emergent phenomenon, LLMs have demonstrated near-human-level intelligence in language processing [15, 87]. Simultaneously, researchers have been attempting to develop MLLMs by integrating multimodal encoders and decoders into LLMs [20, 40, 63, 50, 82, 83]. From the initial MLLMs that could only understand multimodal input signals [58, 60] to later versions supporting the generation of multimodal contents [83, 82, 41, 89, 103], MLLMs have shown powerful capabilities and a broader range of applications. Among all modalities, the integration of vision, known as visual MLLM, has received the most extensive research and application [28, 79, 57, 65]. The latest MLLM research has not only achieved both understanding and generation of visual content, but also developed more refined, pixel-level visual modeling, including segmentation and editing functions [96, 73, 97, 93, 103].

On the other hand, an increasing body of research indicates that visual tokenization [21, 29, 36, 47, 46] significantly impacts MLLM capabilities in vision tasks. The fundamental approach involves encoding the input visual content into feature representations via a visual encoder (e.g., Clip-VIT [70]) and mapping these to an LLM, thus enabling a language-based LLM to understand vision. The corresponding method involves patchifying the original visual images of various sizes into smaller fixed-size patches [21, 4, 60, 82, 83], treating these as tokens, and encoding each patch/token to obtain corresponding embeddings, which are then fed into the LLM. Subsequent research [36, 29], aiming to further unify the training objectives of language and visual modalities, proposed the introduction of codebook techniques, representing visual elements as codebooks. This allows visual training to be treated similarly to language training, i.e., conducting *next token prediction* [29]. Unfortunately, whether in the above visual encoding or tokenization techniques, there is a significant bottleneck of MLLM performance: the integrity of visual semantic units, either visual objects or compositional regions, is compromised during the patchifying process. This results in a less effective semantic alignment between vision and language within the LLM. This paper is the first to propose a solution to this problem, introducing a novel Semantic Equivalent Tokenization for MLLM.

In addition, this work is also related to scene decomposition [90, 68, 62], which involves segmenting a scene into objects. Typically, these methods use a fixed number of query tokens [39, 84] and apply cross-attention [90, 69] to aggregate visual features implicitly. However, this fixed-token approach may not only correspond to the actual visual content but also requires complex network architectures [8, 27] and extensive data for optimization. When combined with LLMs, such complexity significantly increases computational resource demands. Conversely, we learn a dynamic number of semantic objects and do not require complex model structures for optimization, thereby enhancing resource efficiency and providing a more adaptable solution for integrating visual and language modalities.

## 5 Conclusion

In this paper, we present a semantic equivalent tokenization (**SeTok**) to enhance the semantic alignment between vision and text. Technically, we propose a dynamic clustering mechanism to automatically group the visual features into a variable number of semantic complete visual

tokens. Then we equip an MLLM with SeTok and further propose a 3-stage training strategy. After training, our model showcases notable performance on a broad range of comprehension, generation, segmentation, and editing tasks, demonstrating our method’s efficacy.

## References

- [1] Jean-Baptiste Alayrac, Jeff Donahue, Pauline Luc, Antoine Miech, Iain Barr, Yana Hasson, Karel Lenc, Arthur Mensch, Katherine Millican, Malcolm Reynolds, Roman Ring, Eliza Rutherford, Serkan Cabi, Tengda Han, Zhitao Gong, Sina Samangooei, Marianne Monteiro, Jacob L. Menick, Sebastian Borgeaud, Andy Brock, Aida Nematzadeh, Sahand Sharifzadeh, Mikolaj Binkowski, Ricardo Barreira, Oriol Vinyals, Andrew Zisserman, and Karén Simonyan. Flamingo: a visual language model for few-shot learning. In *Proceedings of the NeurIPS*, 2022. 6, 7
- [2] Peter Anderson, Xiaodong He, Chris Buehler, Damien Teney, Mark Johnson, Stephen Gould, and Lei Zhang. Bottom-up and top-down attention for image captioning and visual question answering. In *Proceedings of the CVPR*, pages 6077–6086, 2018. 1
- [3] Jinze Bai, Shuai Bai, Shusheng Yang, Shijie Wang, Sinan Tan, Peng Wang, Junyang Lin, Chang Zhou, and Jingren Zhou. Qwen-vl: A frontier large vision-language model with versatile abilities. *CoRR*, abs/2308.12966, 2023. 5, 6
- [4] Rohan Bavishi, Erich Elsen, Curtis Hawthorne, Maxwell Nye, Augustus Odena, Arushi Somani, and Sağnak Taşırlar. Introducing our multimodal models, 2023. URL <https://www.adept.ai/blog/fuyu-8b>. 9
- [5] Daniel Bolya, Cheng-Yang Fu, Xiaoliang Dai, Peizhao Zhang, Christoph Feichtenhofer, and Judy Hoffman. Token merging: Your vit but faster. In *The Eleventh International Conference on Learning Representations, ICLR 2023, Kigali, Rwanda, May 1-5, 2023*, 2023. 2
- [6] Tim Brooks, Aleksander Holynski, and Alexei A. Efros. Instructpix2pix: Learning to follow image editing instructions. In *IEEE/CVF Conference on Computer Vision and Pattern Recognition, CVPR 2023, Vancouver, BC, Canada, June 17-24, 2023*, pages 18392–18402, 2023. 5, 19
- [7] Tim Brooks, Aleksander Holynski, and Alexei A Efros. Instructpix2pix: Learning to follow image editing instructions. In *Proceedings of the IEEE/CVF Conference on Computer Vision and Pattern Recognition*, pages 18392–18402, 2023. 1, 6
- [8] Mathilde Caron, Piotr Bojanowski, Armand Joulin, and Matthijs Douze. Deep clustering for unsupervised learning of visual features. In *Computer Vision - ECCV 2018 - 15th European Conference, Munich, Germany, September 8-14, 2018, Proceedings, Part XIV*, volume 11218 of *Lecture Notes in Computer Science*, pages 139–156, 2018. 9
- [9] Guiming Hardy Chen, Shunian Chen, Ruifei Zhang, Junying Chen, Xiangbo Wu, Zhiyi Zhang, Zhihong Chen, Jianquan Li, Xiang Wan, and Benyou Wang. Allava: Harnessing gpt4v-synthesized data for A lite vision-language model. *CoRR*, abs/2402.11684, 2024. 5, 19
- [10] Jun Chen, Deyao Zhu, Xiaoqian Shen, Xiang Li, Zechun Liu, Pengchuan Zhang, Raghuraman Krishnamoorthi, Vikas Chandra, Yunyang Xiong, and Mohamed Elhoseiny. Minigt-v2: large language model as a unified interface for vision-language multi-task learning. *arXiv preprint arXiv:2310.09478*, 2023. 5
- [11] Keqin Chen, Zhao Zhang, Weili Zeng, Richong Zhang, Feng Zhu, and Rui Zhao. Shikra: Unleashing multimodal llm’s referential dialogue magic. *CoRR*, abs/2306.15195, 2023. 5
- [12] Lin Chen, Jinsong Li, Xiaoyi Dong, Pan Zhang, Conghui He, Jiaqi Wang, Feng Zhao, and Dahua Lin. Sharegpt4v: Improving large multi-modal models with better captions. *CoRR*, abs/2311.12793, 2023. 5
- [13] Xi Chen, Josip Djolonga, Piotr Padlewski, Basil Mustafa, Soravit Changpinyo, Jialin Wu, Carlos Riquelme Ruiz, Sebastian Goodman, Xiao Wang, Yi Tay, Siamak Shakeri, Mostafa Dehghani, Daniel Salz, Mario Lucic, Michael Tschanen, Arsha Nagrani, Hexiang Hu, Mandar Joshi, Bo Pang, Ceslee Montgomery, Paulina Pietrzyk, Marvin Ritter, A. J. Piergiovanni, Matthias Minderer, Filip Pavetic, Austin Waters, Gang Li, Ibrahim Alabdulmohsin, Lucas Beyer, Julien Amelot, Kenton Lee, Andreas Peter Steiner, Yang Li, Daniel Keysers, Anurag Arnab, Yuanzhong Xu, Keran Rong, Alexander Kolesnikov, Mojtaba Seyedhosseini, Anelia Angelova, Xiaohua Zhai, Neil Houlsby, and Radu Soricut. Pali-x: On scaling up a multilingual vision and language model. *CoRR*, abs/2305.18565, 2023. 5

- [14] Xi Chen, Xiao Wang, Soravit Changpinyo, A. J. Piergiovanni, Piotr Padlewski, Daniel Salz, Sebastian Goodman, Adam Grycner, Basil Mustafa, Lucas Beyer, Alexander Kolesnikov, Joan Puigcerver, Nan Ding, Keran Rong, Hassan Akbari, Gaurav Mishra, Linting Xue, Ashish V. Thapliyal, James Bradbury, and Weicheng Kuo. Pali: A jointly-scaled multilingual language-image model. In *The Eleventh International Conference on Learning Representations, ICLR 2023, Kigali, Rwanda, May 1-5, 2023*, 2023. 5
- [15] Wei-Lin Chiang, Zhuohan Li, Zi Lin, Ying Sheng, Zhanghao Wu, Hao Zhang, Lianmin Zheng, Siyuan Zhuang, Yonghao Zhuang, Joseph E. Gonzalez, Ion Stoica, and Eric P. Xing. Vicuna: An open-source chatbot impressing gpt-4 with 902023. 1, 5, 9
- [16] Guillaume Couairon, Jakob Verbeek, Holger Schwenk, and Matthieu Cord. Diffedit: Diffusion-based semantic image editing with mask guidance. In *Proceedings of the ICLR, 2023*. 1
- [17] Wenliang Dai, Junnan Li, Dongxu Li, Anthony Meng Huat Tiong, Junqi Zhao, Weisheng Wang, Boyang Li, Pascale Fung, and Steven C. H. Hoi. Instructblip: Towards general-purpose vision-language models with instruction tuning. In *Advances in Neural Information Processing Systems 36: Annual Conference on Neural Information Processing Systems 2023, NeurIPS 2023, New Orleans, LA, USA, December 10-16, 2023*, 2023. 5, 6
- [18] Roberto Dessì, Michele Bevilacqua, Eleonora Gualdoni, Nathanaël Carraz Rakotonirina, Francesca Franzon, and Marco Baroni. Cross-domain image captioning with discriminative finetuning. In *Proceedings of the CVPR*, pages 6935–6944, 2023. 1
- [19] Runpei Dong, Chunrui Han, Yuang Peng, Zekun Qi, Zheng Ge, Jinrong Yang, Liang Zhao, Jianjian Sun, Hongyu Zhou, Haoran Wei, Xiangwen Kong, Xiangyu Zhang, Kaisheng Ma, and Li Yi. Dreamllm: Synergistic multimodal comprehension and creation. *CoRR*, abs/2309.11499, 2023. 1, 6
- [20] Runpei Dong, Chunrui Han, Yuang Peng, Zekun Qi, Zheng Ge, Jinrong Yang, Liang Zhao, Jianjian Sun, Hongyu Zhou, Haoran Wei, et al. Dreamllm: Synergistic multimodal comprehension and creation. *arXiv preprint arXiv:2309.11499*, 2023. 5, 9
- [21] Alexey Dosovitskiy, Lucas Beyer, Alexander Kolesnikov, Dirk Weissenborn, Xiaohua Zhai, Thomas Unterthiner, Mostafa Dehghani, Matthias Minderer, Georg Heigold, Sylvain Gelly, Jakob Uszkoreit, and Neil Houlsby. An image is worth 16x16 words: Transformers for image recognition at scale. In *Proceedings of the ICLR, 2021*. 1, 9
- [22] Mingjing Du, Shifei Ding, and Hongjie Jia. Study on density peaks clustering based on k-nearest neighbors and principal component analysis. *Knowl. Based Syst.*, 99:135–145, 2016. 3
- [23] Martin Engelcke, Oiwi Parker Jones, and Ingmar Posner. GENESIS-V2: inferring unordered object representations without iterative refinement. In *Advances in Neural Information Processing Systems 34: Annual Conference on Neural Information Processing Systems 2021, NeurIPS 2021, December 6-14, 2021, virtual*, pages 8085–8094, 2021. 2, 3
- [24] Patrick Esser, Robin Rombach, and Björn Ommer. Taming transformers for high-resolution image synthesis. In *Proceedings of the CVPR*, pages 12873–12883, 2021. 1
- [25] Chaoyou Fu, Peixian Chen, Yunhang Shen, Yulei Qin, Mengdan Zhang, Xu Lin, Zhenyu Qiu, Wei Lin, Jinrui Yang, Xiawu Zheng, Ke Li, Xing Sun, and Rongrong Ji. MME: A comprehensive evaluation benchmark for multimodal large language models. *CoRR*, abs/2306.13394, 2023. 6
- [26] Tsu-Jui Fu, Wenze Hu, Xianzhi Du, William Yang Wang, Yinfei Yang, and Zhe Gan. Guiding instruction-based image editing via multimodal large language models. *CoRR*, abs/2309.17102, 2023. 6, 8
- [27] Wouter Van Gansbeke, Simon Vandenhende, Stamatios Georgoulis, and Luc Van Gool. Unsupervised semantic segmentation by contrasting object mask proposals. In *2021 IEEE/CVF International Conference on Computer Vision, ICCV 2021, Montreal, QC, Canada, October 10-17, 2021*, pages 10032–10042, 2021. 9
- [28] Peng Gao, Jiaming Han, Renrui Zhang, Ziyi Lin, Shijie Geng, Aojun Zhou, Wei Zhang, Pan Lu, Conghui He, Xiangyu Yue, et al. Llama-adapter v2: Parameter-efficient visual instruction model. *arXiv preprint arXiv:2304.15010*, 2023. 9
- [29] Yuying Ge, Yixiao Ge, Ziyun Zeng, Xintao Wang, and Ying Shan. Planting a SEED of vision in large language model. *CoRR*, abs/2307.08041, 2023. 5, 6, 9
- [30] Yash Goyal, Tejas Khot, Aishwarya Agrawal, Douglas Summers-Stay, Dhruv Batra, and Devi Parikh. Making the V in VQA matter: Elevating the role of image understanding in visual question answering. *Int. J. Comput. Vis.*, 127(4):398–414, 2019. 5, 19

- [31] Joakim Bruslund Haurum, Sergio Escalera, Graham W. Taylor, and Thomas B. Moeslund. Which tokens to use? investigating token reduction in vision transformers. In *IEEE/CVF International Conference on Computer Vision, ICCV 2023 - Workshops, Paris, France, October 2-6, 2023*, pages 773–783, 2023. 7
- [32] Byeongho Heo, Song Park, Dongyoon Han, and Sangdoon Yun. Rotary position embedding for vision transformer. *CoRR*, abs/2403.13298, 2024. 4
- [33] Edward J. Hu, Yelong Shen, Phillip Wallis, Zeyuan Allen-Zhu, Yuanzhi Li, Shean Wang, Lu Wang, and Weizhu Chen. Lora: Low-rank adaptation of large language models. In *Proceedings of the ICLR*, 2022. 5, 18
- [34] Drew A Hudson and Christopher D Manning. Gqa: A new dataset for real-world visual reasoning and compositional question answering. In *Proceedings of the IEEE/CVF conference on computer vision and pattern recognition*, pages 6700–6709, 2019. 5, 19
- [35] Peng Jin, Ryuichi Takanobu, Caiwan Zhang, Xiaochun Cao, and Li Yuan. Chat-univi: Unified visual representation empowers large language models with image and video understanding. *CoRR*, abs/2311.08046, 2023. 2
- [36] Yang Jin, Kun Xu, Kun Xu, Liwei Chen, Chao Liao, Jianchao Tan, Quzhe Huang, Bin Chen, Chenyi Lei, An Liu, Chengru Song, Xiaoqiang Lei, Di Zhang, Wenwu Ou, Kun Gai, and Yadong Mu. Unified language-vision pretraining in LLM with dynamic discrete visual tokenization. *CoRR*, abs/2309.04669, 2023. 5, 9
- [37] Sahar Kazemzadeh, Vicente Ordonez, Mark Matten, and Tamara L. Berg. Referitgame: Referring to objects in photographs of natural scenes. In *Proceedings of the 2014 Conference on Empirical Methods in Natural Language Processing, EMNLP 2014, October 25-29, 2014, Doha, Qatar, A meeting of SIGDAT, a Special Interest Group of the ACL*, pages 787–798, 2014. 5, 19
- [38] Alexander Kirillov, Eric Mintun, Nikhila Ravi, Hanzi Mao, Chloé Rolland, Laura Gustafson, Tete Xiao, Spencer Whitehead, Alexander C. Berg, Wan-Yen Lo, Piotr Dollár, and Ross B. Girshick. Segment anything. *CoRR*, abs/2304.02643, 2023. 4, 19
- [39] Alexander Kirillov, Eric Mintun, Nikhila Ravi, Hanzi Mao, Chloe Rolland, Laura Gustafson, Tete Xiao, Spencer Whitehead, Alexander C Berg, Wan-Yen Lo, et al. Segment anything. *arXiv preprint arXiv:2304.02643*, 2023. 1, 9
- [40] Jing Yu Koh, Daniel Fried, and Russ Salakhutdinov. Generating images with multimodal language models. In *Advances in Neural Information Processing Systems 36: Annual Conference on Neural Information Processing Systems 2023, NeurIPS 2023, New Orleans, LA, USA, December 10 - 16, 2023*, 2023. 5, 6, 9
- [41] Jing Yu Koh, Daniel Fried, and Russ R Salakhutdinov. Generating images with multimodal language models. *Advances in Neural Information Processing Systems*, 36, 2023. 9
- [42] Ranjay Krishna, Yuke Zhu, Oliver Groth, Justin Johnson, Kenji Hata, Joshua Kravitz, Stephanie Chen, Yannis Kalantidis, Li-Jia Li, David A. Shamma, Michael S. Bernstein, and Li Fei-Fei. Visual genome: Connecting language and vision using crowdsourced dense image annotations. *Int. J. Comput. Vis.*, 123(1):32–73, 2017. 5, 19
- [43] Xin Lai, Zhuotao Tian, Yukang Chen, Yanwei Li, Yuhui Yuan, Shu Liu, and Jiaya Jia. LISA: reasoning segmentation via large language model. *CoRR*, abs/2308.00692, 2023. 6
- [44] Hugo Laurençon, Léo Tronchon, Matthieu Cord, and Victor Sanh. What matters when building vision-language models?, 2024. 17
- [45] Junnan Li, Dongxu Li, Silvio Savarese, and Steven C. H. Hoi. BLIP-2: bootstrapping language-image pre-training with frozen image encoders and large language models. In *Proceedings of the ICML*, pages 19730–19742, 2023. 4, 5, 6
- [46] Xiangtai Li, Ansheng You, Zhen Zhu, Houlong Zhao, Maoke Yang, Kuiyuan Yang, Shaohua Tan, and Yunhai Tong. Semantic flow for fast and accurate scene parsing. In *Computer Vision–ECCV 2020: 16th European Conference, Glasgow, UK, August 23–28, 2020, Proceedings, Part 1 16*, pages 775–793. Springer, 2020. 9
- [47] Xiangtai Li, Henghui Ding, Wenwei Zhang, Haobo Yuan, Guangliang Cheng, Pang Jiangmiao, Kai Chen, Ziwei Liu, and Chen Change Loy. Transformer-based visual segmentation: A survey. *arXiv pre-print*, 2023. 9



- [48] Xiangtai Li, Haobo Yuan, Wei Li, Henghui Ding, Size Wu, Wenwei Zhang, Yining Li, Kai Chen, and Chen Change Loy. Omg-seg: Is one model good enough for all segmentation? *CoRR*, abs/2401.10229, 2024. [4](#)
- [49] Xiangtai Li, Haobo Yuan, Wei Li, Henghui Ding, Size Wu, Wenwei Zhang, Yining Li, Kai Chen, and Chen Change Loy. Omg-seg: Is one model good enough for all segmentation? *arXiv preprint arXiv:2401.10229*, 2024. [1](#)
- [50] Yanwei Li, Yuechen Zhang, Chengyao Wang, Zhisheng Zhong, Yixin Chen, Ruihang Chu, Shaoteng Liu, and Jiaya Jia. Mini-gemini: Mining the potential of multi-modality vision language models. *CoRR*, abs/2403.18814, 2024. [5](#), [6](#), [8](#), [9](#)
- [51] Yifan Li, Yifan Du, Kun Zhou, Jinpeng Wang, Wayne Xin Zhao, and Ji-Rong Wen. Evaluating object hallucination in large vision-language models. In *Proceedings of the EMNLP*, pages 292–305, 2023. [6](#)
- [52] Yuheng Li, Haotian Liu, Qingyang Wu, Fangzhou Mu, Jianwei Yang, Jianfeng Gao, Chunyuan Li, and Yong Jae Lee. Gligen: Open-set grounded text-to-image generation. In *Proceedings of the IEEE/CVF Conference on Computer Vision and Pattern Recognition*, pages 22511–22521, 2023. [1](#)
- [53] Weixin Liang, Yanhao Jiang, and Zixuan Liu. GraphVQA: Language-guided graph neural networks for graph-based visual question answering. In *Proceedings of the Third Workshop on Multimodal Artificial Intelligence*, pages 79–86, June 2021. [5](#)
- [54] Bin Lin, Yang Ye, Bin Zhu, Jiayi Cui, Munan Ning, Peng Jin, and Li Yuan. Video-llava: Learning united visual representation by alignment before projection. *CoRR*, abs/2311.10122, 2023. [1](#)
- [55] Tsung-Yi Lin, Michael Maire, Serge J. Belongie, James Hays, Pietro Perona, Deva Ramanan, Piotr Dollár, and C. Lawrence Zitnick. Microsoft COCO: common objects in context. In *Computer Vision - ECCV 2014 - 13th European Conference, Zurich, Switzerland, September 6-12, 2014, Proceedings, Part V*, volume 8693 of *Lecture Notes in Computer Science*, pages 740–755, 2014. [4](#), [19](#)
- [56] Chang Liu, Henghui Ding, and Xudong Jiang. Gres: Generalized referring expression segmentation. In *Proceedings of the IEEE/CVF Conference on Computer Vision and Pattern Recognition*, pages 23592–23601, 2023. [5](#), [6](#)
- [57] Fangyu Liu, Guy Emerson, and Nigel Collier. Visual spatial reasoning. *Transactions of the Association for Computational Linguistics*, 11:635–651, 2023. [9](#)
- [58] Haotian Liu, Chunyuan Li, Yuheng Li, and Yong Jae Lee. Improved baselines with visual instruction tuning. *CoRR*, abs/2310.03744, 2023. [5](#), [6](#), [9](#), [19](#)
- [59] Haotian Liu, Chunyuan Li, Qingyang Wu, and Yong Jae Lee. Visual instruction tuning. In *Advances in Neural Information Processing Systems 36: Annual Conference on Neural Information Processing Systems 2023, NeurIPS 2023, New Orleans, LA, USA, December 10 - 16, 2023*, 2023. [5](#), [18](#), [19](#)
- [60] Haotian Liu, Chunyuan Li, Qingyang Wu, and Yong Jae Lee. Visual instruction tuning. *CoRR*, abs/2304.08485, 2023. [9](#)
- [61] Yuan Liu, Haodong Duan, Yuanhan Zhang, Bo Li, Songyang Zhang, Wangbo Zhao, Yike Yuan, Jiaqi Wang, Conghui He, Ziwei Liu, Kai Chen, and Dahua Lin. Mmbench: Is your multi-modal model an all-around player? *CoRR*, abs/2307.06281, 2023. [6](#)
- [62] Francesco Locatello, Dirk Weissenborn, Thomas Unterthiner, Aravindh Mahendran, Georg Heigold, Jakob Uszkoreit, Alexey Dosovitskiy, and Thomas Kipf. Object-centric learning with slot attention. In *Advances in Neural Information Processing Systems 33: Annual Conference on Neural Information Processing Systems 2020, NeurIPS 2020, December 6-12, 2020, virtual*, 2020. [9](#)
- [63] Jiasen Lu, Christopher Clark, Sangho Lee, Zichen Zhang, Savva Khosla, Ryan Marten, Derek Hoiem, and Aniruddha Kembhavi. Unified-io 2: Scaling autoregressive multimodal models with vision, language, audio, and action. *CoRR*, abs/2312.17172, 2023. [5](#), [6](#), [9](#)
- [64] Pan Lu, Liang Qiu, Jiaqi Chen, Tanglin Xia, Yizhou Zhao, Wei Zhang, Zhou Yu, Xiaodan Liang, and Song-Chun Zhu. Iconqa: A new benchmark for abstract diagram understanding and visual language reasoning. In *Proceedings of the Neural Information Processing Systems Track on Datasets and Benchmarks 1, NeurIPS Datasets and Benchmarks 2021, December 2021, virtual*, 2021. [5](#)
- [65] Pan Lu, Liang Qiu, Jiaqi Chen, Tony Xia, Yizhou Zhao, Wei Zhang, Zhou Yu, Xiaodan Liang, and Song-Chun Zhu. Iconqa: A new benchmark for abstract diagram understanding and visual language reasoning. *arXiv preprint arXiv:2110.13214*, 2021. [9](#)

- [66] Junhua Mao, Jonathan Huang, Alexander Toshev, Oana Camburu, Alan L. Yuille, and Kevin Murphy. Generation and comprehension of unambiguous object descriptions. In *2016 IEEE Conference on Computer Vision and Pattern Recognition, CVPR 2016, Las Vegas, NV, USA, June 27-30, 2016*, pages 11–20, 2016. [19](#)
- [67] Kenneth Marino, Mohammad Rastegari, Ali Farhadi, and Roozbeh Mottaghi. OK-VQA: A visual question answering benchmark requiring external knowledge. In *IEEE Conference on Computer Vision and Pattern Recognition, CVPR 2019, Long Beach, CA, USA, June 16-20, 2019*, pages 3195–3204, 2019. [5](#), [19](#)
- [68] Dantong Niu, Xudong Wang, Xinyang Han, Long Lian, Roei Herzig, and Trevor Darrell. Unsupervised universal image segmentation. *CoRR*, abs/2312.17243, 2023. [9](#)
- [69] Lu Qi, Jason Kuen, Tiancheng Shen, Jiuxiang Gu, Wenbo Li, Weidong Guo, Jiaya Jia, Zhe Lin, and Ming-Hsuan Yang. High quality entity segmentation. In *IEEE/CVF International Conference on Computer Vision, ICCV 2023, Paris, France, October 1-6, 2023*, pages 4024–4033, 2023. [9](#)
- [70] Alec Radford, Jong Wook Kim, Chris Hallacy, Aditya Ramesh, Gabriel Goh, Sandhini Agarwal, Girish Sastry, Amanda Askell, Pamela Mishkin, Jack Clark, Gretchen Krueger, and Ilya Sutskever. Learning transferable visual models from natural language supervision. In *Proceedings of the ICML*, pages 8748–8763, 2021. [9](#)
- [71] Alec Radford, Jong Wook Kim, Chris Hallacy, Aditya Ramesh, Gabriel Goh, Sandhini Agarwal, Girish Sastry, Amanda Askell, Pamela Mishkin, Jack Clark, et al. Learning transferable visual models from natural language supervision. In *International conference on machine learning*, pages 8748–8763. PMLR, 2021. [1](#)
- [72] Aditya Ramesh, Prafulla Dhariwal, Alex Nichol, Casey Chu, and Mark Chen. Hierarchical text-conditional image generation with clip latents. *arXiv preprint arXiv:2204.06125*, 2022. [1](#)
- [73] Hanoona Rasheed, Muhammad Maaz, Sahal Shaji, Abdelrahman Shaker, Salman Khan, Hisham Cholakkal, Rao M Anwer, Erix Xing, Ming-Hsuan Yang, and Fahad S Khan. Glamm: Pixel grounding large multimodal model. *arXiv preprint arXiv:2311.03356*, 2023. [9](#)
- [74] Hanoona Abdul Rasheed, Muhammad Maaz, Sahal Shaji Mullappilly, Abdelrahman Shaker, Salman H. Khan, Hisham Cholakkal, Rao Muhammad Anwer, Erix Xing, Ming-Hsuan Yang, and Fahad Shahbaz Khan. Glamm: Pixel grounding large multimodal model. *CoRR*, abs/2311.03356, 2023. [8](#)
- [75] Zhongwei Ren, Zhicheng Huang, Yunchao Wei, Yao Zhao, Dongmei Fu, Jiashi Feng, and Xiaojie Jin. Pixellm: Pixel reasoning with large multimodal model. *arXiv preprint arXiv:2312.02228*, 2023. [6](#)
- [76] Robin Rombach, Andreas Blattmann, Dominik Lorenz, Patrick Esser, and Björn Ommer. High-resolution image synthesis with latent diffusion models. In *Proceedings of the CVPR*, pages 10674–10685, 2022. [1](#), [4](#), [6](#)
- [77] Christoph Schuhmann, Romain Beaumont, Richard Vencu, Cade Gordon, Ross Wightman, Mehdi Cherti, Theo Coombes, Aarush Katta, Clayton Mullis, Mitchell Wortsman, Patrick Schramowski, Srivatsa Kundurthy, Katherine Crowson, Ludwig Schmidt, Robert Kaczmarczyk, and Jenia Jitsev. LAION-5B: an open large-scale dataset for training next generation image-text models. In *Advances in Neural Information Processing Systems 35: Annual Conference on Neural Information Processing Systems 2022, NeurIPS 2022, New Orleans, LA, USA, November 28 - December 9, 2022*, 2022. [4](#), [19](#)
- [78] Dustin Schwenk, Apoorv Khandelwal, Christopher Clark, Kenneth Marino, and Roozbeh Mottaghi. A-OKVQA: A benchmark for visual question answering using world knowledge. In *Computer Vision - ECCV 2022 - 17th European Conference, Tel Aviv, Israel, October 23-27, 2022, Proceedings, Part VIII*, volume 13668 of *Lecture Notes in Computer Science*, pages 146–162, 2022. [5](#), [19](#)
- [79] Dustin Schwenk, Apoorv Khandelwal, Christopher Clark, Kenneth Marino, and Roozbeh Mottaghi. A-okvqa: A benchmark for visual question answering using world knowledge. In *European Conference on Computer Vision*, pages 146–162. Springer, 2022. [9](#)
- [80] Piyush Sharma, Nan Ding, Sebastian Goodman, and Radu Soricut. Conceptual captions: A cleaned, hypernymed, image alt-text dataset for automatic image captioning. In *Proceedings of the ACL*, pages 2556–2565, 2018. [4](#), [19](#)
- [81] Shelly Sheynin, Adam Polyak, Uriel Singer, Yuval Kirstain, Amit Zohar, Oron Ashual, Devi Parikh, and Yaniv Taigman. Emu edit: Precise image editing via recognition and generation tasks. *CoRR*, abs/2311.10089, 2023. [6](#)

- [82] Quan Sun, Yufeng Cui, Xiaosong Zhang, Fan Zhang, Qiyong Yu, Zhengxiong Luo, Yueze Wang, Yongming Rao, Jingjing Liu, Tiejun Huang, and Xinlong Wang. Generative multimodal models are in-context learners. *CoRR*, abs/2312.13286, 2023. 5, 6, 8, 9
- [83] Quan Sun, Qiyong Yu, Yufeng Cui, Fan Zhang, Xiaosong Zhang, Yueze Wang, Hongcheng Gao, Jingjing Liu, Tiejun Huang, and Xinlong Wang. Generative pretraining in multimodality. *CoRR*, abs/2307.05222, 2023. 5, 9
- [84] Teppei Suzuki. Clustering as attention: Unified image segmentation with hierarchical clustering. *CoRR*, abs/2205.09949, 2022. 9
- [85] Hao Tan and Mohit Bansal. LXMERT: learning cross-modality encoder representations from transformers. In *Proceedings of the 2019 Conference on Empirical Methods in Natural Language Processing and the 9th International Joint Conference on Natural Language Processing, EMNLP-IJCNLP 2019, Hong Kong, China, November 3-7, 2019*, pages 5099–5110, 2019. 5
- [86] Hao Tan, Franck Dernoncourt, Zhe Lin, Trung Bui, and Mohit Bansal. Expressing visual relationships via language. In *Proceedings of the 57th Conference of the Association for Computational Linguistics, ACL 2019, Florence, Italy, July 28- August 2, 2019, Volume 1: Long Papers*, pages 1873–1883, 2019. 6
- [87] Rohan Taori, Ishaan Gulrajani, Tianyi Zhang, Yann Dubois, Xuechen Li, Carlos Guestrin, Percy Liang, and Tatsunori B. Hashimoto. Stanford alpaca: An instruction-following llama model. 2023. URL [https://github.com/tatsu-lab/stanford\\_alpaca](https://github.com/tatsu-lab/stanford_alpaca). 1, 9
- [88] Jianzong Wu, Xiangtai Li, Chenyang Si, Shangchen Zhou, Jingkang Yang, Jiangning Zhang, Yining Li, Kai Chen, Yunhai Tong, Ziwei Liu, et al. Towards language-driven video inpainting via multimodal large language models. *arXiv preprint arXiv:2401.10226*, 2024. 1
- [89] Shengqiong Wu, Hao Fei, Leigang Qu, Wei Ji, and Tat-Seng Chua. Next-gpt: Any-to-any multimodal LLM. *CoRR*, abs/2309.05519, 2023. 9
- [90] Tao Yang, Yuwang Wang, Yan Lu, and Nanning Zheng. Visual concepts tokenization. In *Advances in Neural Information Processing Systems 35: Annual Conference on Neural Information Processing Systems 2022, NeurIPS 2022, New Orleans, LA, USA, November 28 - December 9, 2022*, 2022. 9
- [91] Xu Yang, Kaihua Tang, Hanwang Zhang, and Jianfei Cai. Auto-encoding scene graphs for image captioning. In *Proceedings of the CVPR*, pages 10685–10694, 2019. 1
- [92] Zhao Yang, Jiaqi Wang, Yansong Tang, Kai Chen, Hengshuang Zhao, and Philip HS Torr. Lavt: Language-aware vision transformer for referring image segmentation. In *Proceedings of the IEEE/CVF Conference on Computer Vision and Pattern Recognition*, pages 18155–18165, 2022. 1, 5
- [93] Haoxuan You, Haotian Zhang, Zhe Gan, Xianzhi Du, Bowen Zhang, Zirui Wang, Liangliang Cao, Shih-Fu Chang, and Yinfei Yang. Ferret: Refer and ground anything anywhere at any granularity. *CoRR*, abs/2310.07704, 2023. 9
- [94] Alex Young, Bei Chen, Chao Li, Chengen Huang, Ge Zhang, Guanwei Zhang, Heng Li, Jiangcheng Zhu, Jianqun Chen, Jing Chang, Kaidong Yu, Peng Liu, Qiang Liu, Shawn Yue, Senbin Yang, Shiming Yang, Tao Yu, Wen Xie, Wenhao Huang, Xiaohui Hu, Xiaoyi Ren, Xinyao Niu, Pengcheng Nie, Yuchi Xu, Yudong Liu, Yue Wang, Yuxuan Cai, Zhenyu Gu, Zhiyuan Liu, and Zonghong Dai. Yi: Open foundation models by 01.ai. *CoRR*, abs/2403.04652, 2024. 5
- [95] Weihao Yu, Zhengyuan Yang, Linjie Li, Jianfeng Wang, Kevin Lin, Zicheng Liu, Xinchao Wang, and Lijuan Wang. Mm-vet: Evaluating large multimodal models for integrated capabilities. *CoRR*, abs/2308.02490, 2023. 6
- [96] Yuqian Yuan, Wentong Li, Jian Liu, Dongqi Tang, Xinjie Luo, Chi Qin, Lei Zhang, and Jianke Zhu. Osprey: Pixel understanding with visual instruction tuning. *CoRR*, abs/2312.10032, 2023. 8, 9
- [97] Ao Zhang, Wei Ji, and Tat-Seng Chua. Next-chat: An LMM for chat, detection and segmentation. *CoRR*, abs/2311.04498, 2023. 6, 9
- [98] Ao Zhang, Liming Zhao, Chen-Wei Xie, Yun Zheng, Wei Ji, and Tat-Seng Chua. Next-chat: An lmm for chat, detection and segmentation. *arXiv preprint arXiv:2311.04498*, 2023. 5, 6
- [99] Ao Zhang, Hao Fei, Yuan Yao, Wei Ji, Li Li, Zhiyuan Liu, and Tat-Seng Chua. Vpgrans: Transfer visual prompt generator across llms. *Advances in Neural Information Processing Systems*, 36, 2024. 1

- [100] Bowen Zhang, Shuyang Gu, Bo Zhang, Jianmin Bao, Dong Chen, Fang Wen, Yong Wang, and Baining Guo. Styleswin: Transformer-based GAN for high-resolution image generation. In *Proceedings of the CVPR*, pages 11294–11304, 2022. [1](#)
- [101] Kai Zhang, Lingbo Mo, Wenhui Chen, Huan Sun, and Yu Su. Magicbrush: A manually annotated dataset for instruction-guided image editing. In *Advances in Neural Information Processing Systems 36: Annual Conference on Neural Information Processing Systems 2023, NeurIPS 2023, New Orleans, LA, USA, December 10 - 16, 2023*. [6](#), [8](#)
- [102] Kai Zhang, Lingbo Mo, Wenhui Chen, Huan Sun, and Yu Su. Magicbrush: A manually annotated dataset for instruction-guided image editing. *Advances in Neural Information Processing Systems*, 36, 2024. [1](#), [6](#)
- [103] Tao Zhang, Xiangtai Li, Hao Fei, Haobo Yuan, Shengqiong Wu, Shunping Ji, Change Loy Chen, and Shuicheng Yan. Omg-llava: Bridging image-level, object-level, pixel-level reasoning and understanding. *arXiv preprint*, 2024. [9](#)
- [104] Xueyan Zou, Jianwei Yang, Hao Zhang, Feng Li, Linjie Li, Jianfeng Wang, Lijuan Wang, Jianfeng Gao, and Yong Jae Lee. Segment everything everywhere all at once. *Advances in Neural Information Processing Systems*, 36, 2024. [6](#)



## A Ethic Statement

This work aims to build semantic equivalence tokenization to segment input images into semantic complete tokens to enhance the MLLMs in vision understanding, generation, segmentation, and editing capabilities. Here we discuss all the possible potential impacts of the proposed MLLM, SETOKIM.

**Use of Generative Content** The SETOKIM, limited by the quantity of fine-tuning data and the quality of the base models, may generate some low-quality content. Also, as a generative model, the LLM will produce hallucinated content in multimodal formats that may be harmful to society. We have reminded users to interpret the results with caution. Anyone who uses this LLM should obey the rules in a license. And also commercial use of our system is not allowed.

**Data Privacy and Security** Our research utilizes datasets that are either publicly available or collected with explicit consent. We adhere to strict data privacy and security protocols to protect the information and ensure it is used solely for this research.

**Bias Mitigation** Recognizing the potential for bias in AI models, particularly in vision-language tasks, we rigorously test our tokenizer across diverse datasets. This approach is designed to identify and mitigate biases that may affect the model’s performance or lead to unfair outcomes in its applications.

## B Limitation

While SETOKIM has achieved further improvements across various language-driven vision tasks, becoming a zero-shot general specialist, it still faces several limitations.

**Model Scale.** The evaluation of our model is currently constrained to configurations with 7B and 13B parameters. As shown in [44], the performance of MLLMs is limited by the scale of the core backbone LLM. Despite the impressive results achieved, the potential benefits of employing significantly larger models, such as 65B or 130B, are worth exploring in future studies.

**The resolution of Image.** Regarding image resolution, our model currently handles images up to a maximum resolution of 336x336. While there have been improvements in understanding visually fine-grained content, challenges remain when processing higher-resolution images. Therefore, enhancing the model to support images of any resolution could further improve its visual perception capabilities.

**Hallucination.** Although our model has made some progress in mitigating hallucination through fine-grained vision-language alignment, as demonstrated in experiments on the POPE dataset, the issue of hallucinations remains inevitable. This area continues to pose challenges and is a crucial aspect for future exploration and enhancement.

## C Detailed Clustering Algorithm

The formal clustering algorithm is described in Algorithm 1. Specifically, a scope  $c = [0, 1]^{h \times w}$  is initialized to a matrix of ones  $1^{h \times w}$  to track the degree to which visual embeddings have been assigned to clusters. In addition, the seed scores are initialized by combining the local density in Eq.(1) and distance in Eq.(2) to perform the selection of visual embeddings. At each iteration, a single embedding vector  $x_{i,j}$  is selected at the spatial location  $(i, j)$  which corresponds to the argmax of the element-wise multiplication of the seed scores and the current scope. This ensures that cluster seeds are sampled from pixel embeddings that have not yet been assigned to clusters. An alpha mask  $\alpha_i [0, 1]^{h \times w}$  is computed as the distance between the cluster seed embedding  $x_{i,j}$  and all individual pixel embeddings according to a distance kernel  $\varphi$ . The output of the kernel  $\varphi$  is one if two embeddings are identical and decreases to zero as the distance between a pair of embeddings increases. The associated attention mask  $M_k$  is obtained by the element-wise multiplication of the alpha masks by the current scope to ensure that the final set of attention masks is normalized. The scope is then updated by an element-wise multiplication with the complement of the alpha masks.

This process is repeated until a stopping condition is satisfied, at which point the final scope is added as an additional mask to explain any remaining embeddings.

---

**Algorithm 1** Clustering Algorithm

---

**Require:** visual embeddings  $\mathbf{X} \in \mathbb{R}^{h \times w \times d}$   
**Ensure:** masks  $\mathbf{M} \in \mathbb{R}^{h \times w \times k}$  with  $\mathbf{M}_{1:k} \in [0, 1]^{h \times w}$

- 1: Initialize: masks  $\mathbf{M} = \emptyset$ , scope  $c = 1^{H \times W}$ , seed scores  $s \in \mathbb{R}^{h \times w}$
- 2: **while** not StopCondition( $\mathbf{M}$ ) **do**
- 3:      $(i, j) = \arg \max(s > 0)$
- 4:      $\alpha = \text{DistanceKernel}(\mathbf{X}, (i, j))$
- 5:      $\mathbf{M}.\text{append}(s \odot \alpha)$
- 6:      $s = s \odot (1 - \alpha)$
- 7: **end while**
- 8:  $\mathbf{M}.\text{append}(s)$

---

## D Detailed Experiments Settings

### D.1 Implementation Details

Our model utilizes two types of vision encoders: Vit-G/14-336 and ConvNext-XXL. For the language model backbone, we choose Vicuna-v1.5 in both the 7B and 13B versions. The cluster merger within our architecture comprises two blocks, each equipped with a multi-head self-attention mechanism consisting of two heads, a feed-forward layer, and layers for residual connections and normalization. Regarding feature mapping, we initialize the backbone with the pre-trained BERT-base model. Additionally, SD v1.5 is used to set the initial parameters for the U-Net. This integrated approach ensures a robust foundation for processing and interpreting multimodal inputs. We employ LoRA [33] and partial parameter fine-tuning to optimize the model. Here, we detail the training data utilized at each stage in Table 6.

### D.2 Training Receipt

In Table 7, we list the detailed hyper-parameters setting at three stages. All the training of SETOKIM is conducted on  $16 \times$  A800 (80G) GPUs.

## E Extended Experimental Analysis

**Ablation Study.** Here, we conduct an ablation study to assess the design advantages of our model, with the results presented in Table 8. Initially, removing the position embedding from each cluster significantly impaired performance in visual understanding and editing tasks. Subsequently, replacing the cluster merger with an average visual representation for each cluster also led to a modest decline in fine-grained visual performance.

**The Adaption of SeTok.** To investigate whether our proposed semantic-equivalent tokenizer could be transferred to established MLLMs, thereby enhancing their performance across various tasks, we select models that cater to varying resolutions: Emu-1 supporting  $224 \times 224$ , LLaVA-v1.5 supporting  $336 \times 336$ , and Yi-VL supporting  $448 \times 448$ . Then, these MLLMs are incorporated with our semantic-equivalent tokenizer behind the input connector of these existing models, where each token represents the average of tokens within a cluster. Furthermore, we sample 10k instruction data from LLaVA-150k [59] to fine-tune the original and modified models. The experimental results are presented in Table 9. Firstly, a marked improvement across various tasks can be observed after the application of SeTok, indicating the effectiveness and necessity of aligning visual tokens semantically with text tokens. Furthermore, while the increase in resolution typically requires a higher number of visual tokens in the original MLLMs, the introduction of clustering results in a more consistent number of tokens being fed into the LLM. This consistency is crucial as the attention computation in LLMs exhibits a quadratic relationship concerning the token length; thus, this sparsification can accelerate the training process and significantly reduce computational costs during inference.

Table 6: The training data used in our experiments.

	Name	Brief Description
<b>Stage-I</b>	CC3M [80]	3.3M image-text pairs from the web.
	LAION-AESTHETICS [77]	LAION-Aesthetics is a subsets collection from LAION-5B with high visual quality.
	MSCOCO2017 [55]	COCO is a large-scale object detection, segmentation, and captioning dataset.
	SAM-1B [38]	1 Billion (SA-1B) is a dataset designed for training general-purpose object segmentation models from open-world images
<b>Stage-II</b>	LLaVA-filter CC3M dataset [58]	LLaVA Visual Instruct CC3M Pretrain 595K is a subset of CC3M dataset, filtered with a more balanced concept coverage distribution.
	ALLaVA-pretraining [9]	A dataset is constructed by leveraging the superb GPT-4V to generate captions and complex reasoning QA pairs.
	InstructPix2Pix [6]	A large scale instructin-based image editing dataset.
<b>Stage-III</b>	LLaVA-150K [59]	LLaVA Visual Instruct 150K is a set of GPT-generated multimodal instruction-following data.
	ALLaVA-instruction [9]	A dataset is constructed by leveraging the superb GPT-4V to generate captions and complex reasoning QA pairs.
	VQA <sup>v2</sup> [30]	VQA is a dataset containing open-ended questions about images, which require an understanding of vision, language, and commonsense knowledge to answer.
	GQA [34]	GQA features compositional questions over real-world images.
	OKVQA [67]	OK-VQA is a dataset for visual question answering that requires methods that can draw upon outside knowledge to answer questions
	AOKVQA [78]	AOKVQA is a new knowledge-based visual question answering benchmark
	RefCOCO+/g [37, 66]	RefCOCO+/g dataset is a referring expression segmentation (RES) dataset used for tasks related to understanding natural language expressions that refer to specific objects in images.
VG [42]	Visual Genome is a dataset, a knowledge base, an ongoing effort to connect structured image concepts to language	

Table 7: Training recipes for SETOKIM. The three training stages are introduced in Section 2.2. Stage-I: Tokenizer Pretraining, Stage-II: Multimodal Pretraining, Stage-III: End-to-end Instruction Tuning.

Configuration	Stage-I	Stage-II	Stage-III
Optimizer	AdamW	AdamW	AdamW
Learning Rate	0.001&0.004	0.004	0.0005
Weight Decay	0.001	0.001	0.001
Training Epochs	1	1	1
Warmup Ratio	0.1	0.1	0.1
Learning Rate Scheduler	Cosine	Cosine	Cosine
Batch Size Per GPU	32	32	32
Maximum Token Length	77	2048	2048

**The Impact of Visual Encoder.** Here, we analyze the impact of using the same clustering mechanism on the effectiveness of vision encoders. Initially, as demonstrated in Figure 7(a), we observe that the transformer-based vision encoder exhibits superior performance in both understanding and generating visual content. Upon investigating the reasons, we found that visual features obtained from the ConvNext model do not easily differentiate focal points, as shown in Figure 7(b). This may be due to the local receptive fields in convolutional networks, resulting in each feature focusing solely on

	VQA <sup>v2</sup> ↑	GQA ↑	MagicBrush ↓	Resolution	#Token	VQA <sup>v2</sup>	Flickr30K	GQA
LLaVA-1.5	78.5	62.0	-	Emu-1-7B	256	57.8	80.9	46.5
<b>SETOKIM</b>	83.9	67.2	5.7	+ <b>SeTok</b>	17*	58.6	39.6	48.3
w/o PE	80.3 (-3.6)	62.1 (-5.1)	10.2(+4.5)	LLaVA-V1.5-7B	576	80.2	83.2	54.0
w/o Cluster Merger	82.7 (-1.2)	64.0 (-3.2)	7.7 (+2.5)	+ <b>SeTok</b>	19*	81.2	65.6	55.8
				Yi-VL-6B	1024	75.3	73.5	58.7
				+ <b>SeTok</b>	22*	77.1	61.8	60.5

Table 8: Ablation study. ‘w/o PE’ denotes we remove the position embedding for each visual token when integrating the **SeTok** and fine-tuning on the small instruction dataset. ‘w/o Cluster Merger’ means we average tokens within each cluster to represent the corresponding number of visual tokens fed into LLM. \*: the average number of visual tokens.

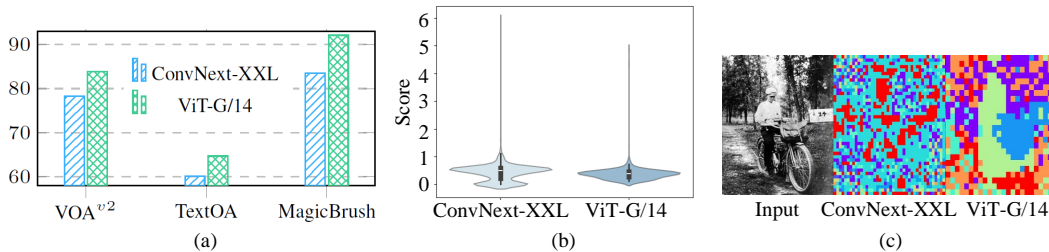


Figure 7: Comparative analysis of CNN-based (e.g., ConvNext-XXL) and transformer-based (e.g., ViT-G/14) vision encoders: (a) performance on three distinct tasks, (b) distribution of cluster possibility scores for visual features, and (c) clustering outcomes with a fixed set of 10 clusters.



Figure 8: The image reconstruction results from visual tokens by the denoising U-Net.

its own region and highly dispersed scores. In contrast, the score distribution of the ViT-G/14 is much more compact, implying a greater consistency or reliability in the scores it produces. Furthermore, employing the same number of clusters for both visual feature groups, further visualization of the clustering outcomes in Figure 7(c) reveals that clusters based on convolution are quite arbitrary and do not discern object-level information. Conversely, clusters derived from transformer-based models delineate object contours, enabling the generation of more precise object-centric visual tokens, and leading to better performance in various multimodal tasks.

**The quality of Reconstruction.** In Figure 8, we visualize some reconstructed examples by the trained denoising U-Net. It can be seen that, given the tokenized visual tokens, the original input images can be successfully recovered. The reconstructed examples exhibit a high degree of reconstruction of the method.